organoids

MDPI

Article

Pyrvinium Pamoate and BCL-XL Inhibitors Act Synergistically to Kill Patient-Derived Colorectal Adenoma Organoids

Maree C. Faux [1,2,3,*,†], Chenkai Ma [4], Serena R. Kane [1,2], Andre Samson [2,5], Yumiko Hirokawa [1,2], Ilka Priebe [6], Leah Cosgrove [6], Rajvinder Singh [7], Michael Christie [8], Gregor Brown [9], Kim Y. C. Fung [4] and Antony W. Burgess [1,2,3,*]

1 Personalised Oncology Division, The Walter and Eliza Hall Institute of Medical Research, 1G Royal Parade, Parkville, VIC 3052, Australia
2 Department of Medical Biology, University of Melbourne, Parkville, VIC 3052, Australia
3 Department of Surgery, RMH, University of Melbourne, Parkville, VIC 3052, Australia
4 CSIRO Health and Biosecurity, 160 Hawkesbury Rd., Westmead, NSW 2145, Australia; kim.fung@csiro.au (K.Y.C.F.)
5 Inflammation Division, The Walter and Eliza Hall Institute of Medical Research, 1G Royal Parade, Parkville, VIC 3052, Australia
6 CSIRO Health and Biosecurity, Kintore Ave, Adelaide, SA 5000, Australia
7 Lyell McEwin Hospital, Elizabeth Vale, SA 5112, Australia
8 Department of Pathology, Royal Melbourne Hospital, Parkville, VIC 3052, Australia
9 Alfred Health, 55 Commercial Rd., Melbourne, VIC 3004, Australia
* Correspondence: maree.faux@mcri.edu.au (M.C.F.); tburgess@wehi.edu.au (A.W.B.); Tel.: +613-83-416-200 (M.C.F.); +613-934-525-55 (A.W.B.); Fax: +613-83-416-212 (M.C.F.); +613-934-708-52 (A.W.B.)
† Current address: Murdoch Children's Research Institute, 50 Flemington Road, Parkville, VIC 3052, Australia.

Abstract

Current systemic therapies for advanced colorectal cancer (CRC) have limited efficacy, so more effective strategies for the treatment and prevention of CRC are needed. The majority of colorectal cancers are initiated by mutations in Wnt signalling pathway genes, including mutations in the *APC* gene, which result in a truncated APC protein and lead to excess signalling from β-catenin and the formation of pre-cancerous adenomas. The aim of this study was to determine if targeting the Wnt pathway in combination with pro-apoptotic mimetics altered the proliferative capacity or viability of human colorectal adenoma cells. Patient-derived colorectal adenoma organoid cultures were established from colon adenoma tissue collected by colonoscopy and recapitulated the histopathology of primary colorectal adenoma tissue. The growth of colorectal adenoma organoids is inhibited by the Wnt-signalling antagonist pyrvinium pamoate (PP) and a pro-apoptotic inhibitor of BCL-XL but not BCL-2 (venetoclax) or MCL-1 inhibitors. At low concentrations, the PP and the BCL-XL inhibitor combination demonstrated potent synergy and induced apoptosis in *APC*-defective patient-derived adenoma organoids, even in the presence of oncogenic *KRAS* or *BRAF* mutations, providing a new strategy for colon cancer prevention.

Keywords: intestinal organoids; adenoma; adenomatous polyposis coli; colorectal cancer

Academic Editor: Roberto Benelli

Received: 10 April 2025
Revised: 30 April 2025
Accepted: 30 June 2025
Published: 2 July 2025

Citation: Faux, M.C.; Ma, C.; Kane, S.R.; Samson, A.; Hirokawa, Y.; Priebe, I.; Cosgrove, L.; Singh, R.; Christie, M.; Brown, G.; et al. Pyrvinium Pamoate and BCL-XL Inhibitors Act Synergistically to Kill Patient-Derived Colorectal Adenoma Organoids. *Organoids* **2025**, *4*, 15. https://doi.org/10.3390/organoids4030015

1. Introduction

Colorectal cancer (CRC) is one of the most common cancers worldwide and is a leading cause of cancer-related death [1]. CRC often arises from pre-cancerous adenomas that acquire additional mutations that eventually lead to invasive carcinomas [2,3]. Pre-cancerous

adenomas can be successfully detected and removed during regular colonoscopy surveillance [4]; however, colonoscopy screening is expensive, time-consuming, and invasive. Despite extensive colon cancer screening programs, the number of cases of CRC continues to increase worldwide [5,6]. A prevention strategy designed to kill pre-cancerous adenoma stem cells would provide a means to reduce the incidence of CRC.

Most CRCs are initiated by mutations in the *adenomatous polyposis coli (APC)* gene, which leads to aberrant Wnt signalling [7,8]. The majority of adenomas, including lateral spreading adenomas, contain *APC* mutations [9,10]. A second subtype of CRC arising from sessile serrated polyps accounts for up to 25% of sporadic disease and is characterised by mutations in the *BRAF* gene (i.e., $BRAF^{V600E}$) that activate the MAPK pathway [11,12].

Despite compelling evidence for the role of Wnt signalling in colon adenoma initiation and CRC, there are currently no Wnt pathway signalling inhibitors approved for treating CRC. An FDA-approved anthelmintic drug, pyrvinium pamoate (PP), has been shown to inhibit the Wnt pathway, reducing the levels of activated β-catenin [13,14]. Although PP has been reported to increase the sensitivity of cancer cells to chemotherapeutic drugs [15], it also inhibits other biochemical pathways [16–20]. We have recently discovered that the combination of PP and a Bcl2-family inhibitor (ABT737 or ABT263) inhibits the growth of CRC cells in vitro and in CRC xenografts in mice [21]. Furthermore, we have observed that *Apc*-mutant mouse adenoma size is decreased upon treatment with PP+ABT263 [22]. We, therefore, hypothesised that a Wnt inhibitor in combination with a pro-apoptotic drug could be used to kill pre-cancerous human adenoma cells.

In this study, we aimed to assess the sensitivity of patient-derived colon adenoma organoids to Wnt signalling inhibitors [13,14,23,24] and Bcl-2 family inhibitors. The use of patient-derived organoids allows us to test drug sensitivities directly on each patient's cells and provides an opportunity to predict an individual's response to specific drug combinations. From colon adenoma tissue collected by colonoscopy, we established a panel of living colorectal adenoma organoids. The adenoma organoids recapitulated the characteristics of patient-derived colon adenoma tissue. When tested as single agents, both PP and a BCL-XL inhibitor were effective in inhibiting adenoma organoid growth, whereas other Wnt inhibitors (tankyrase and IWP2) and BCL-2 family inhibitors (to BCL-2 and MCL-1) were ineffective. Significantly, killing was more efficient when PP and a BCL-XL inhibitor were used in combination. These results suggest that a new drug combination of Wnt antagonist and pro-apoptotic inhibitor could be an effective strategy for killing colon adenomas and preventing CRC.

2. Materials and Methods

2.1. Ethics and Consent

This study was conducted in accordance with the Declaration of Helsinki and the NH&MRC Statement on Ethical Conduct in Human Research, and the protocol was approved by The Alfred Health Human Research Ethics Committee (LR195-14, 29.08.2014), the Walter and Eliza Hall Institute Human Research Ethics Committee (HREC14/17), and the Central Adelaide Local Health Network Human Research Ethics Committee (HREC/19/CALHN/13). All patients provided informed consent. Adenoma tissue (clinically sporadic) and adjacent normal epithelial from the adenoma were obtained from consenting patients undergoing colonoscopy at the Epworth Hospital, Richmond, Australia, or the Lyell McEwin Hospital, Adelaide, Australia. The patient cohort was restricted to patients with lesions that were both suitable for EMR (Endoscopic Mucosal Resection) and large enough to be able to retain tissue for research purposes as well as routine diagnosis (i.e., >20 mm). In some cases, a number of polyp pieces were collected. Patient information, including clinical characteristics, is presented in Table 1.

Table 1. Patient clinical information.

Patient	Age	Sex	Adenoma Type	Adenoma Site	Number of Adenomas	Adenoma Size &	Differentiation	Invasive Carcinoma	Passage Organoid Cryopreserved
009	74	F	1. tubulovillous 2. benign fibrous tissue 3. tubulovillous	1. caecum 2. transverse colon 3. transverse colon	1. multiple 2. 3 3. multiple	1. 20 × 12 × 9 mm 2. 2 to 3 mm 3. 17 × 16 × 7 mm	1. high-grade dysplasia 2. nil 3. high-grade dysplasia	No	1. >P1 2. not cultured 3. not cultured
013	81	M	tubulovillous	rectum	1	16 × 15 × 9 mm	low-grade dysplasia	No	P0
015	70	M	1. traditional serrated 2. tubular	1. proximal ascending colon 2. mid ascending colon	1. multiple 2. 1	1. 20 × 12 × 10 mm 2. 3 mm	1. low-grade dysplasia 2. low-grade dysplasia	No	1. >P1 2. not cultured
016	79	F	tubular	caecum	multiple	12 × 4 × 2 mm	low-grade dysplasia	No	>P1
017	64	F	tubulovillous	ascending colon	multiple	27 × 22 × 15 mm	low- and high-grade dysplasia	No	>P1
018	59	M	tubulovillous	ileocaecal valve	multiple	16 × 11 × 5 mm	high-grade dysplasia *	No	>P1
020	76	F	traditional sessile serrated	1. Ileocaecal valve 2. caecum 3. ascending colon 4. hepatic flexure	4	1. 14 × 10 × 6 mm 2. 10 mm 3. 21 × 11 × 1 mm 4. 14 × 6 × 4 mm	1. low-grade dysplasia 2. low-grade dysplasia 3. no cytological dysplasia 4. no cytological dysplasia	Not stated	1. >P1 2. not cultured 3. not cultured 4. not cultured
021	65	F	tubulovillous	hepatic flexure	multiple	1 to 5 mm	low-grade dysplasia	Not stated	>P1
022	55	M	tubulovillous	caecum	multiple	5 to 15 mm	low-grade dysplasia	No	>P1
024	70	M	1. sessile serrated 2. tubular	1. hepatic flexure 2. transverse colon	1. 1 2. 2	1. 2 to 6 mm 2. 2 to 7 mm	low-grade dysplasia	No	1. >P1 2. not cultured
025	68	F	sessile serrated	hepatic flexure	2	8 and 10 mm	no cytologic dysplasia	Not stated	P0
026	70	F	tubulovillous	ileocaecal valve	multiple	12 × 2 × 7 mm	low-grade dysplasia	No	P0
027	50	F	tubulovillous	transverse colon	multiple	15 × 10 × 9 mm	low-grade dysplasia	No	P0
029	59	F	tubular	caecum	not stated	Not stated	low grade and high grade	No	P0
035	na	na	sessile tubulovillous	caecum	1	50 mm	moderately differentiated adenocarcinoma	Yes	n/a
039	74	M	villous	rectum	not stated	Not stated	high-grade dysplasia ^	No	>P1
040	72	M	tubulovillous	rectum	multiple	18 × 12 × 12 mm	low-grade dysplasia	No	>P1
041	75	M	villous	caecum	1	30 × 20 × 12 mm	high-grade dysplasia	No	>P1

Table 1. *Cont.*

Patient	Age	Sex	Adenoma Type	Adenoma Site	Number of Adenomas	Adenoma Size [&]	Differentiation	Invasive Carcinoma	Passage Organoid Cryopreserved
042	71	M	tubulovillous	ascending colon	2	1. 50 × 50 × 15 mm 2. 22 × 14 × 13 mm	high-grade dysplasia	No	1. >P1 2. not cultured
044	64	F	tubulovillous	sigmoid colon	1	26 × 13 × 9 mm	low- and high-grade dysplasia	No	>P1
045	62	F	tubulovillous	transverse colon	multiple	18 × 13 × 10 mm	low- and high-grade dysplasia	No	>P1
048	63	F	tubulovillous	caecum	1	45 × 35 × 5 mm	low-grade dysplasia	No	>P1
049	62	F	1. sessile serrated 2. tubular	1. transverse colon 2. rectum	1. 1 2. 2	1. 15 × 10 × 2 mm 2. 12 × 8 × 2 mm	1. no sessile dysplasia 2. low-grade dysplasia	No	>P1
050	59	F	tubulovillous	caecum	1	45 × 35 × 10 mm	low-grade dysplasia	No	>P1
051	73	F	tubular	sigmoid colon	1	18 mm	low-grade dysplasia	No	P0
052	88	F	1. tubular 2. villous	1. ascending colon 2. rectosigmoid	1. 1 1. 1	1. 2 to 4 mm 2. 60 × 30 × 5 mm	1. low-grade dysplasia 2. low-grade dysplasia	No	1. P0 2. not cultured
053	80	M	sessile serrated	caecum	multiple	1 to 10 mm	focal high-grade dysplasia	No	>P1
036 [a]	80	M	villous	transverse colon	not stated	40 mm	low-grade dysplasia	No	>P1
051 [a]	66	M	sessile serrated adenoma	hepatic flexure	not stated	80 mm	no dysplasia	No	>P1
054 [a]	67	M	tubulovillous	hepatic flexure	not stated	40 mm	low-grade dysplasia	No	>P1
056 [a]	72	M	tubulovillous	transverse colon	not stated	50 mm	low-grade dysplasia	No	>P1
057 [a]	74	M	tubulovillous adenoma	splenic flexure	not stated	30 mm	low-grade dysplasia	No	>P1
058 [a]	53	M	sessile serrated adenoma	caecum	not stated	30 mm	no dysplasia	No	>P1

[&] Adenoma size up to xx mm. Number of adenomas refers to the number of polyp pieces collected and is reported as multiple if >3. Organoid passage denotes if organoid cultures were cryopreserved at P0 or greater than P1. The majority of organoids were passaged over >4 passages. * Moderately differentiated adenocarcinoma arising in association with a tubulovillous adenoma with high-grade dysplasia; ^ specimen 1 rectal polyp, 2 polyp base invasive poorly differentiated mucinous adenocarcinoma; n/a not applicable, tissue not available. Tissue samples were collected from the Epworth Hospital, Richmond, Australia, or the Lyell McEwin Hospital, Adelaide, Australia [a].

2.2. Establishing Colorectal Adenoma Organoids

Adenoma tissue samples were collected in ice-cold phosphate-buffered saline (PBS) and treated with 0.04% sodium hypochlorite in PBS for 5 min. Samples were washed with ice-cold PBS and finely minced with scissors before incubation in digestion mix (0.1 mg/mL Dispase (Life Technologies Thermo Fischer Scientific, Waltham, MA, USA 17105-041) and 200 U collagenase IV (Life Technologies Thermo Fischer Scientific, Waltham, MA, USA 17104019) in DME/F12 (Thermo Fischer Scientific, Waltham, MA, USA), processing using a gentle MACS^{TM} Dissociator (Miltenyi Biotec, Macquarie Park NSW, Australia 130-093-235), and incubation at 37 °C for 10 min. Processing with the tissue dissociator and incubation at 37 °C for 10 min was repeated 3 times. The tissue fragments were washed with DME/F12 and filtered through a 70 µm cell strainer (Bio-strategy, Tullamarine, VIC, Australia BDAA352350), washed with DME/F12 containing 1% BSA (Sigma-Aldrich Merck Life Science, Bayswater, VIC, Australia), and pelleted by centrifugation (300× *g*, 3 min). The cell pellet was resuspended in Organoid Growth Medium I (IntestiCult Organoid Growth Medium (Human) (Stemcell Technologies, Vancouver, BC, Canada, 72308) or Organoid Growth Medium II (DME/F12 containing 100 mM HEPES (Sigma-Aldrich Merck Life Science, Bayswater, VIC, Australia H3375), B27 supplement (LifeTechnologies Thermo Fischer Scientific, Waltham, MA, USA 17504001), N2 supplement (Life Technologies Thermo Fischer Scientific, Waltham, MA, USA 17502001), 50% Wnt3a-conditioned medium (CM) (from Wnt3a-expressing cell line ATCC, CRL-2647), 2% RSpondin2-CM (Fc-tagged recombinant RSpondin2 expressed in 293F cells (a kind gift from Dr. Nadia Kershaw RRID:CVCL_6642 [25]), 10% Noggin-CM (from the Noggin-expressing cell line, a kind gift from Prof. Hans Clevers), 50 ng/mL EGF (PeproTech, Cranbury, NJ, USA 120-43)), 500 nM A83-01 (Tocris Bioscience, Bristol, UK 29-391-0), 10 µM SB202190 (Sigma-Aldrich Merck Life Science, Bayswater, VIC, Australia S7067), 10 µM nicotinamide (Sigma-Aldrich, Merck Life Science, Bayswater, VIC, Australia 72340), 1 mM N-acetyl-L-cysteine (Sigma-Aldrich, Merck Life Science, Bayswater, VIC, Australia A7250)) containing 100 U/mL penicillin-streptomycin (Life Technologies Thermo Fischer Scientific, Waltham, MA, USA 15140122), and a 10 µM Y27632 dihydrochloride Rho Kinase inhibitor (MedChem Express, Monmouth Junction, NJ, USA). Cells were either incubated in dome cultures by suspending in 50% Matrigel and plating in 20 µL domes in a 6-well plate or in suspension containing 5% Matrigel (Corning Bio-strategy, Tullarmarine, VIC, Australia BDAA354234) and plating in 6-well suspension low adherent plates (Interpath, Somerton, VIC, Australia 657185) [26]. For dome cultures, Matrigel domes were allowed to polymerise by incubation at 37 °C for 30 min and were then overlaid with Organoid Growth Medium. Organoids were grown in a CO_2 incubator at 37 °C with 10% CO_2 in Organoid Growth Medium without Y27632.

2.3. Histology and Immunohistochemistry

Primary tissue samples were embedded in O.C.T (Tissue-Tek, Emgrid, Gulfview Heights, SA, Australia 4583) and frozen in an isopropanol bath on dry ice. Organoids were harvested and resuspended in DME/F12 containing 1% BSA and 10 µM Y27632 and incubated on ice for 1 h to allow the Matrigel to melt. The cells were centrifuged at 1500 rpm, washed once with PBS, the cell pellet was resuspended in PBS, and an equal volume of pre-warmed Histo-gel (Richard-Allan Scientific HistoGel^{TM} Specimen Processing Gel, Thermo Fischer Scientific, Waltham, MA, USA) was added. Histo-gel domes (50–70 µL) were plated on pre-cooled glass coverslips and incubated at 4 °C for 15 min before fixation by incubation in 10% formalin. Gel domes were embedded in paraffin. Specimen sections were prepared for hematoxylin and eosin (H&E) and Ki67 staining.

For Ki67 staining, sections were dewaxed and incubated with antibodies to Ki67 (Cell Signalling Technology, Boston, MA, USA #12202, 1:400), followed by incubation with peroxidase-conjugated polymer conjugated to rabbit IgG (Dako Agilent Technologies, Santa Clara, CA, USA K4003). Peroxidase activity was detected by incubation with EnV FLEX HRP Chromagen Substrate (Dako Agilent Technologies, Santa Clara, CA, USA) for 10 min. Stained slides were scanned on a 3D Histech Panoramic Scan II histology scanner (3DHISTECH Ltd., Budapeset, Hungary) and assessed using CaseViewer Software Ver 3.3 (3DHISTECH Ltd.).

2.4. Immunofluorescence and Confocal Microscopy

For immunofluorescence microscopy, organoids were grown in 6-well suspension low-adherent plates as described above. Organoids were grown for 5–7 days in suspension and then harvested in ice-cold PBS. Organoids were centrifuged at 70× *g* for 5 min at 4 °C and washed with ice-cold PBS to dissolve the remaining Matrigel. The organoids were then fixed, cleared, immunolabelled, and prepared for confocal imaging, as described in [27]. In brief, organoids were fixed by incubation with 4% paraformaldehyde (Electron Microscopy Sciences, Hatfield, PA, USA #15710) in PBS for 45 min at 4 °C and then incubated in 0.1% Tween20 in PBS for 10 min at 4 °C and transferred into a 24-well low-adherent plate. Organoids were blocked in 0.1% Triton X-100 and 0.2% BSA in PBS (OWB) at 4 °C for 15 min and washed with fresh OWB. Organoids were incubated with E-cadherin antibody (BD, Macquarie Park, NSW, Australia, #610182, 1:200) diluted in OWB at 4 °C overnight on a horizontal shaker (60 rpm). Organoids were then washed with three 2 h washes in OWB at 4 °C on a horizontal shaker (60 rpm), and incubated with AlexaFluor 488 anti-mouse IgG (H+L) (Invitrogen Thermo Fischer Scientific, Waltham, MA, USA #A11001, 1:500) and Phalloidin (Molecular Probes Invitrogen Thermo Fischer Scientific, Waltham, MA, USA 1:200) diluted in OWB overnight at 4 °C on a horizontal shaker (60 rpm). Organoids were washed as previously described, incubated with DAPI (Thermo Fischer Scientific, Waltham, MA, USA, #62248, 1:1000), washed again before transferring to a 1.5 mL Eppendorf tube, centrifuged at 70× *g* for 5 min, and OWB aspirated. Organoids were cleared by incubating in a fructose glycerol clearing solution at room temperature for 20 min, and then slides were prepared for confocal imaging. Images were acquired on an Olympus IX81 confocal microscope using Olympus Fluoview Ver.2.1C software. Slice images were exported from Olympus Fluoview Ver.4.2a Viewer software.

For cell death analysis, organoids were seeded in Matrigel domes in 8-well µ-slides (Ibidi DKSH Australia, Tullamarine, VIC, Australia #80826) overlaid with Organoid Growth Medium I. Organoids were grown under humidified 10% CO_2 at 37 °C for 5 days before being treated with PP (1 µM), Bcl-XL inhibitor (0.1 µM), or PP (1 µM) + Bcl-XL inhibitor (0.1 µM). AlexaFluor488-conjugated Annexin V (1:500) (Thermo Fisher Scientific Waltham, MA, USA #A13201), TO-PRO-3 (1:2000; Thermo Fisher Scientific Waltham, MA, USA #T3605), and Hoechst 33342 (1:10,000; ThermoFisher Scientific Waltham, MA, USA #H3570) were added to the cultures immediately prior to imaging. Cells were imaged on an Inverted LSM 880 confocal microscope (Zeiss, Jena, China) with the following specifications: Plan-Apochromat 20×/0.80 air lens, 405, 488, and 633 nm laser lines, Zeiss photomultiplier tube, ZEN black 2.3 SP1 FP3 v14.0 capture software, and ImageJ Ver 1.52p post-acquisition processing software RRID:SCR_003070. Cells were maintained under humidified 5% CO_2 at 37 °C.

2.5. Whole Exome Sequencing (WES) and Genetic Alteration Analysis

Genomic DNA was isolated from snap-frozen OCT samples with the Qiagen DNeasy Blood & Tissue Kit. Matched normal and adenoma (n = 17 patients) tissues were sequenced

on an Illumina HiSeq platform (Australian Genome Research Facility). The exome design used at AGRF was xGen Exome Research Panel v2. After demultiplexing and quality control performed by AGRF, all raw sequencing reads were subjected to trimming the adapters and low-quality reads by Trim Galore (RRID:SCR_011847) with the following settings: -q 20 --length 20 -e 0.1. The GATK4 workflow was adapted for genome alignment and variant calling. Specifically, trimmed reads were subject to BWA-mem for alignment against GRh38 with default settings. Germline variant calling was performed by HaplotypeCaller according to the GATK4 workflow with default settings. Identified variants were annotated by ClinVar using SnpEff (Ver 5.0e) (RRID:SCR_005191). Only pathogenic or likely pathogenic variants noted in "Clinsig" by ClinVar (RRID:SCR_006169) were shortlisted for visualisation. The copy number alteration (CNA) was determined by the CNVkit with the "HMM-germline" argument in the segmentation. As normal matched samples were not available for all patient samples, we aggregated all normal samples as the normal control for the CNA analysis of the samples.

2.6. Adenoma Organoid Drug Sensitivity and Analysis

Organoids were harvested and digested with TrypLE express enzyme (Thermo Fischer Scientific, Waltham, MA, USA #12604013) at 37 °C for 10 min. Cells were washed with DME/F12 containing 1% BSA and resuspended in DME/F12 containing 1% BSA and 10 µM Y27632. The cells were dissociated with a 26G needle to ensure a single cell suspension and collected by centrifugation. Cells were resuspended in Organoid Growth Medium I containing 3% Matrigel and 10 µM Y27632 and seeded in 384-well optical plates (Thermo Fischer Scientific, Waltham, MA, USA #242764) (5000 cells in 40 µL/well). PBS (70 µL/well) was added to wells on the outer edges to prevent evaporation. Cells were grown under humidified 10% CO_2 at 37 °C for 3–7 days to establish organoids.

Drugs were assayed in triplicate in an 8-point 2-, 3-, or 5-fold dilution series in Organoid Growth Medium I with starting concentrations of 1 µM for Pyrvinium Pamoate [14], Mcl-1 inhibitor (MedChemExpress Monmouth Junction, NJ, USA #HY100741/CS-6420 S63845 Lot#25867), Bcl2 inhibitor Venetoclax (MedChemExpress Monmouth Junction, NJ, USA #HY15531/CS-1155 Lot# 3606), 1 µM for tankyrase inhibitor G007.LK [28] (a kind gift from Michael Buchert, Olivier Newton John Cancer Research Institute, Heidelberg, VIC, Australia), and porcupine inhibitor IWP2 [24] (a kind gift from Liz Vincan, University of Melbourne, Parkville, VIC, Australia). The starting concentration for the Bcl-XL inhibitor (MedChemExpress Monmouth Junction, NJ, USA #HY-19741/CS-5565 A-1331852 Lot#24104) was 1 µM for PDA0044 and 0.1 µM for all other samples. DMSO 0.166% (v/v) and 1 µM bortezomib were used as negative and positive controls, respectively. PP and the Bcl-XL inhibitor were incubated by titrating 8-point dilutions of the Bcl-XL inhibitor in a matrix with 8-point dilutions of PP. Adenoma organoids were incubated with drugs for 72 h before the addition of 20 µL CellTiterGlo 3D reagent (Promega, Hawthorn East, VIC, Australia G9683). Plates were shaken at 1000 rpm on an IKA MS3 digital shaker for 5 min and incubated at room temperature for 25 min. Luminescence was measured using an EnVision plate reader (PerkinElmer, Glen Waverly, VIC, Australia). Dose–response curves were plotted as % inhibition compared to maximal growth and were fitted using a sigmoid, exponential, or polynomial function with the curve fit function of the scipy optimise module [29]. The abscissa scale on the growth curves is presented as Log10(10 × drug concentration) nM or Log10(1000 × drug concentration) nM. For 1000 nM, Log10(10 × 1000 nM PP) = 4; for 100 nM, Log10(1000 × 100 nM) = 5. The Bliss scores were calculated [30] and were plotted with Matplotlib Ver 3.2.1 [31] using Python 3.0 (RRID:SCR_008624).

2.7. Statistical Analysis

For statistical analysis for multiple comparison analysis, a one-way ANOVA test was performed with the Bonferroni correction method for multiple comparisons using GraphPad Prism Ver 9 software (GraphPad Software, La Jolla, CA, USA) (RRID:SCR_002798). Statistical analysis for the drug combinations comparison of PP with and without BCL-XL inhibitors was calculated using the R package "drc" Ver 3.0-1 [32]. In brief, each experiment's data was normalised before the dose–response curve model was generated by the four-parameter log-logistic function. Statistical difference was calculated between parameter estimates for the parameter "EC50". For statistical analysis for imaging analysis, a one-way ANOVA test was performed with Tukey's multiple comparison test within GraphPad Prism Ver 9 (GraphPad Software, La Jolla, CA, USA RRID:SCR_002798).

3. Results

3.1. Patient-Derived Adenoma Organoids Display Similar Histological Features to Their Primary Tissue

We derived a panel of 32 adenoma organoids from colon adenoma tissue collected via endoscopy from patients with adenomas (Figure 1). The clinical data from the patient cohort is presented in Table 1 and shows that more than half the samples (n = 17) were tubulovillous adenomas in addition to tubular (n = 4), villous (n = 2), traditional serrated (n = 3), and sessile serrated adenomas (n = 6) at a range of sites, including caecum, hepatic flexure, and rectum. The adenomas mostly demonstrated low-grade dysplasias. There were six patients with adenomas detected at more than one site (Table 1). A living biobank of the patient-derived adenoma organoids (PDAOs) was established in growth media using conditions described by Sato et al. [33] for a normal human colon for downstream analysis (Figure 1A).

It is well documented that organoids derived from normal colon recapitulate the morphology and organisation of the tissue of origin [33,34]. Histological sections of primary adenomas and PDAOs were assessed by a pathologist, and in general, the histology of the adenoma organoids matched the primary tissue with similar morphologies evident in the organoids (Figures 1B,C and S1). Representative samples of the morphology of the organoids used in subsequent drug assays are included. PA044 and PA045 had characteristic tubulovillous morphology consistent with low-grade dysplasia with small, rounded tubules and larger irregular tubules, respectively (Figures 1B and S1A), and the organoids show a corresponding structure with simple tubules (Figures 1B and S1B). The primary adenoma in PDAO053 was a sessile serrated adenoma with typical serrated glandular structures (Figure S1A). The PDAO053 organoids recapitulated the serrated morphology that is evident in the primary tissue (Figure S1B). Proliferative cells were evident throughout the colon adenoma tissue and were maintained in the organoid structures (Figure 1C). The adenoma organoids derived from individual patients show different growth characteristics and structures: the organoids derived from PA044 display smaller clusters compared to larger cyst-like structures from PDAO053 (Figure S1E). Immunostained PDAOs display properly organised intestinal cell layers with polarised apical (actin) and basolateral (E-cadherin) distributions (Figures 1D and S2, Supplemental Movies S1–S3). The adenoma organoids produce multiple crypt-like buds in which E-cadherin is localised at the cell periphery on the basolateral surface, and actin decorates the apical membranes on the internal side of the structure (Figures 1D and S2A, Supplemental Movies S1 and S2). Inverted budding structures with actin staining on the external boundary were also present (Figure S2A,B, Supplemental Movies S2 and S3).

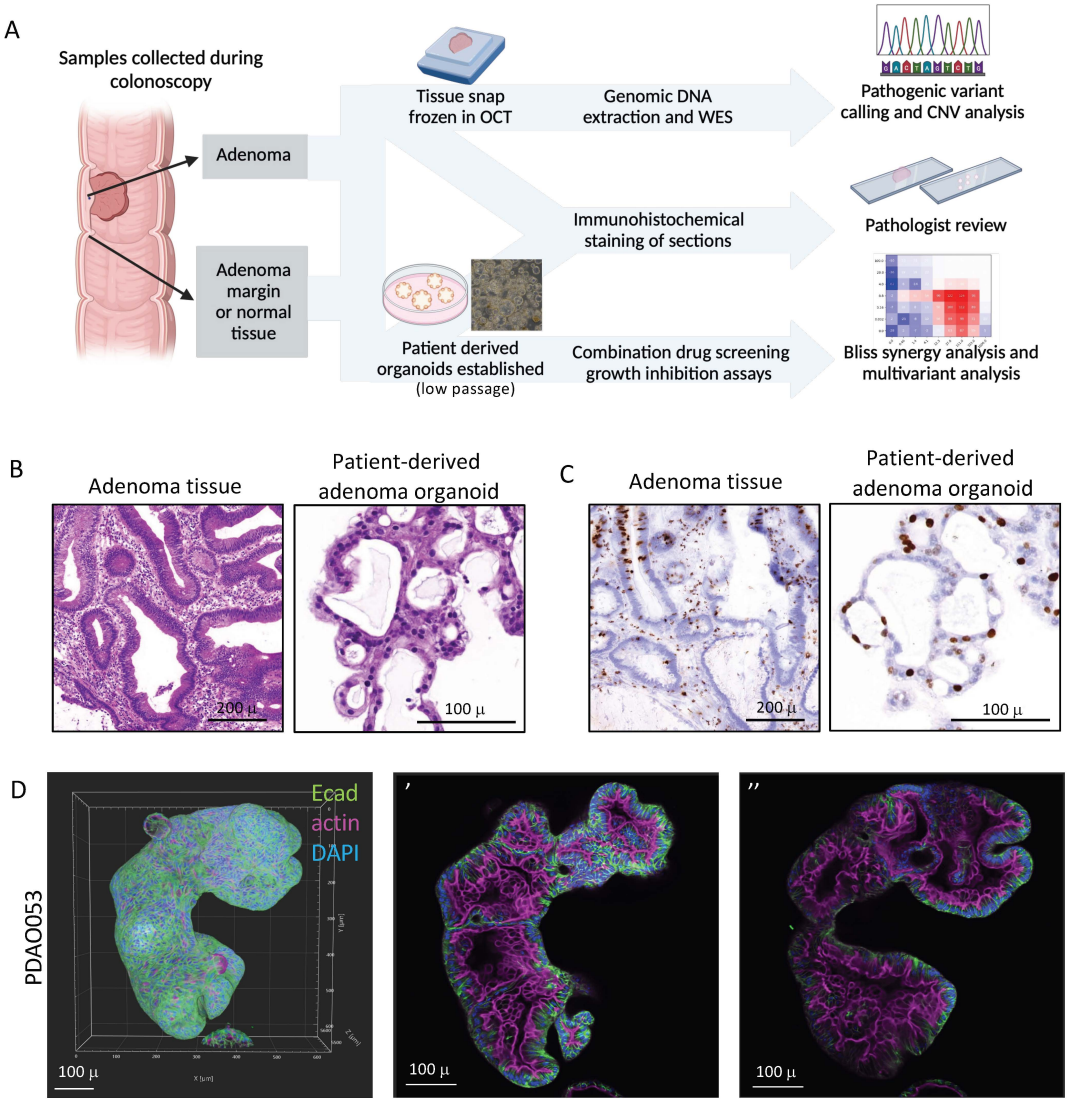

Figure 1. Patient-derived colon adenoma organoids recapitulate the histological features of their primary adenoma tissue. (**A**) Study design schematic (Biorender). (**B**) Haematoxylin and eosin (H&E)-stained histological sections of primary adenoma tissue PA045 and adenoma organoids derived from the same sample. Characteristic tubulovillous morphology and irregular glands are evident. (**C**) Ki67-stained histological sections of primary adenoma tissue PA045 and adenoma organoids derived from the same sample. (**D**) Representative confocal microscopy of patient-derived adenoma organoids. Organoids were fixed and immunostained with antibodies to E-cadherin (green) and co-stained with phalloidin to visualize actin (magenta) and DAPI to visualise the nuclei (blue), and images were collected on an Olympus FV1000 confocal microscope equipped with a 20× lens (Olympus Australia, Mt Waverly, VIC, Australia). Shown are images rendered in Imaris (3D blend mode) and single confocal slices (' slice 43 of 64, '' slice 23 of 64). Scale bars are indicated.

Overall, these data show that the morphology of the adenoma organoids was similar to the respective primary tissue adenomas, suggesting that these PDAOs were appropriate models to use for testing drug sensitivity.

3.2. Genomic Analysis of Colorectal Adenomas

To investigate the genetic alterations of colorectal adenoma, WES was performed for seventeen patient samples, selected as representative samples from each cohort, including ten adenoma/adenoma margin pairs and seven adenoma/matched normal pairs (Figure 2). We identified the most frequent somatic variants as *KRAS* (71%) and *APC* (59%) in patient

adenoma tissue (Supplemental Figure S3), which were absent in patient normal colon (Supplemental Figure S4). We observed mutation patterns in signalling pathways, including WNT, PI3K, and ERBB genes (Figure 2A). We examined copy number alterations (Figure 2B) and found that four adenomas harboured loss of *APC*; these samples had no *APC* mutations (Supplemental Figure S5). Thus, *APC* loss or mutation was present in 77% of adenomas. We also observed copy number gain of *KRAS* and *BRAF* in one and five adenomas, respectively (Figure S5). Of the four samples with no Wnt signalling-associated mutations or *APC* loss, two were sessile polyps, with gain of *BRAF* (P035 and P053). We also investigated copy number gain or loss of BCL2 family members in our cohort and found gain of *BCL2* (one adenoma) and *MCL1* (one adenoma) and *BCL2L1* (BCL-XL) loss (four adenomas) (Supplemental Figure S6). Taken together, the WES of colon adenoma samples indicated mutation and/or loss of *APC*, in addition to mutations and/or copy number gain in *KRAS* or *BRAF*, drives adenoma formation.

3.3. Patient-Derived Adenoma Organoid Sensitivity to Wnt and BCL-2 Family Inhibitors

In order to understand the effects of Wnt inhibition and BCL2-family inhibitors, PDAOs were exposed to Wnt inhibitor pyrvinium (pyrvinium pamoate, PP) and BH3-mimetic drugs that target BCL-2 (venetoclax), BCL-XL, or MCL1 as single agents. The cellular actions of PP are complex, and the direct target(s) have been difficult to establish [35]. Wnt signalling inhibition is one of the proposed cellular actions of PP, as treatment of colorectal cancer cells with PP leads to reduced cytoplasmic β-catenin and Tcf reporter activity [21] and the suppression of Wnt inducible genes [36]. Given the role of aberrant Wnt signalling in driving adenoma formation and CRC, targeting the Wnt pathway with PP is of clinical interest. Representative PDAOs derived from eight patients with colon adenomas were expanded and treated with an increasing dose of PP over 72 h (Figures 3 and S7A–E). Adenoma organoids derived from tissues containing mutations in APC or other Wnt pathway genes would be expected to respond to treatment with Wnt inhibitors [13,21]. Indeed, each of the PDAO samples tested responded to PP with IC50s in the range of 10–150 nM (Figure 3A–C). Inhibition curves were fitted with linear regression analysis and showed up to 80% inhibition at 1 μM. A subset of PDAOs was treated with a tankyrase inhibitor, G007-LK, or a porcupine inhibitor, IWP2 (Supplementary Figure S8). G007-LK is a small molecule inhibitor reported to reduce Wnt/β-catenin signalling by preventing poly (ADP-ribosyl)ation-dependent AXIN degradation, thereby promoting β-catenin destabilisation [28]. The porcupine inhibitor IWP2 prevents Wnt secretion and has been reported to disrupt Wnt signalling [24,37]. However, in contrast to the response to Wnt antagonist PP, the growth of the PDAOs was not affected by G007-LK or IWP2, although both PDAO045 and PDAO050 (*APC* deficient) appear more sensitive to G007-LK compared to PDAO044 with no APC or Wnt defect (Figure S8). There was no difference in drug response between early and later passage, which ranged in our drug assays from Passage (*p*) 2 to P20 (Supplemental Table S1).

Patient-derived CRC organoids have been shown to respond to BCL-2 family inhibitors and show increased sensitivity when these compounds are used in combination [38]. In our experiments, the PDAOs were exquisitely sensitive to the BCL-XL inhibitor but did not respond to either BCL-2 (venetoclax) or MCL-1 inhibitors (Figures 3D–F and S7). The PDAOs show sensitivity to BCL-XL inhibition with IC50s < 10 nM (Figure 3D–G). We compared the mutation and copy number status of the adenomas from WES with response to Wnt signalling and BCL-XL inhibition for eight PDAO samples. *APC* was mutated or lost in seven of the eight PDAO samples, and there was a gain of one copy of *BCL-XL* in four of the eight PDAOs (Figure 3H). Of these, one sample, PDAO044, contained only loss of *BCL-XL* and no identified *APC* or Wnt pathway gene mutation. PDAOs with loss

of *APC* and gain of *BCL-XL* were significantly more sensitive to PP when compared to adenomas with loss of *APC* only (Figure 3I). PDAOs with gain of *BCL-XL* also only showed reduced sensitivity compared to *APC* loss and gain of *BCL-XL*, but it must be noted that our sample size is limited to only one PDAO with gain of *BCL-XL* only, and any drug response differences must be treated cautiously. There was no association with loss of APC or gain of BCL-XL and the PDAO responses to the BCL-XL inhibitor in our cohort of PDAOs (Figure 3J).

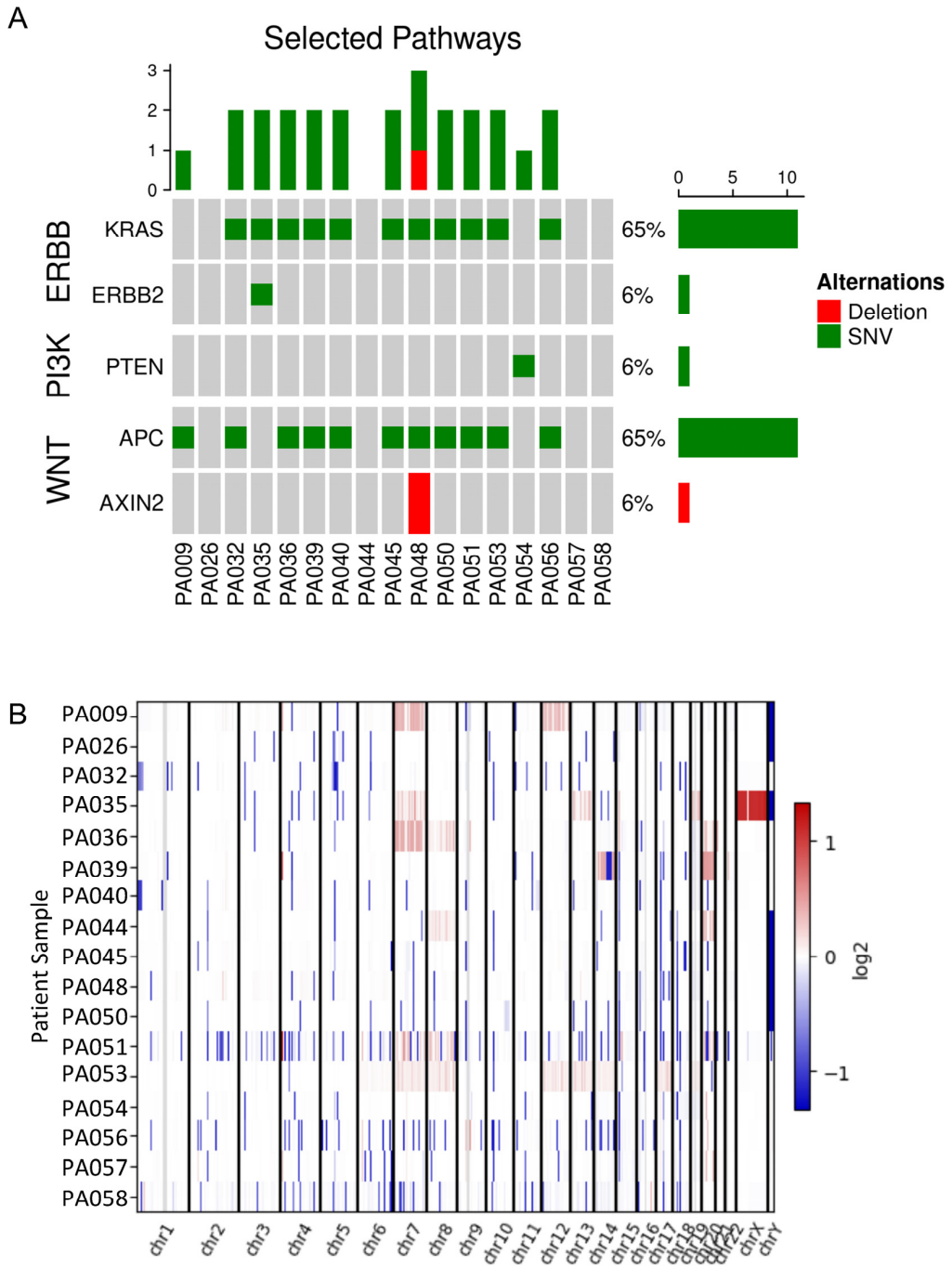

Figure 2. Genetic alteration of patient adenoma samples. (**A**) Oncoplot representation of all somatic variants of WNT, PI3K, and ERBB pathways in individual patient adenomas, including deletions and SNVs. Samples are arranged in columns, with genes labelled along rows. The number of altered genes in selected pathways is shown in the top profile, and the number of samples (percentage) is shown in the plots to the right. (**B**) Heatmap showing the copy number alterations in all samples.

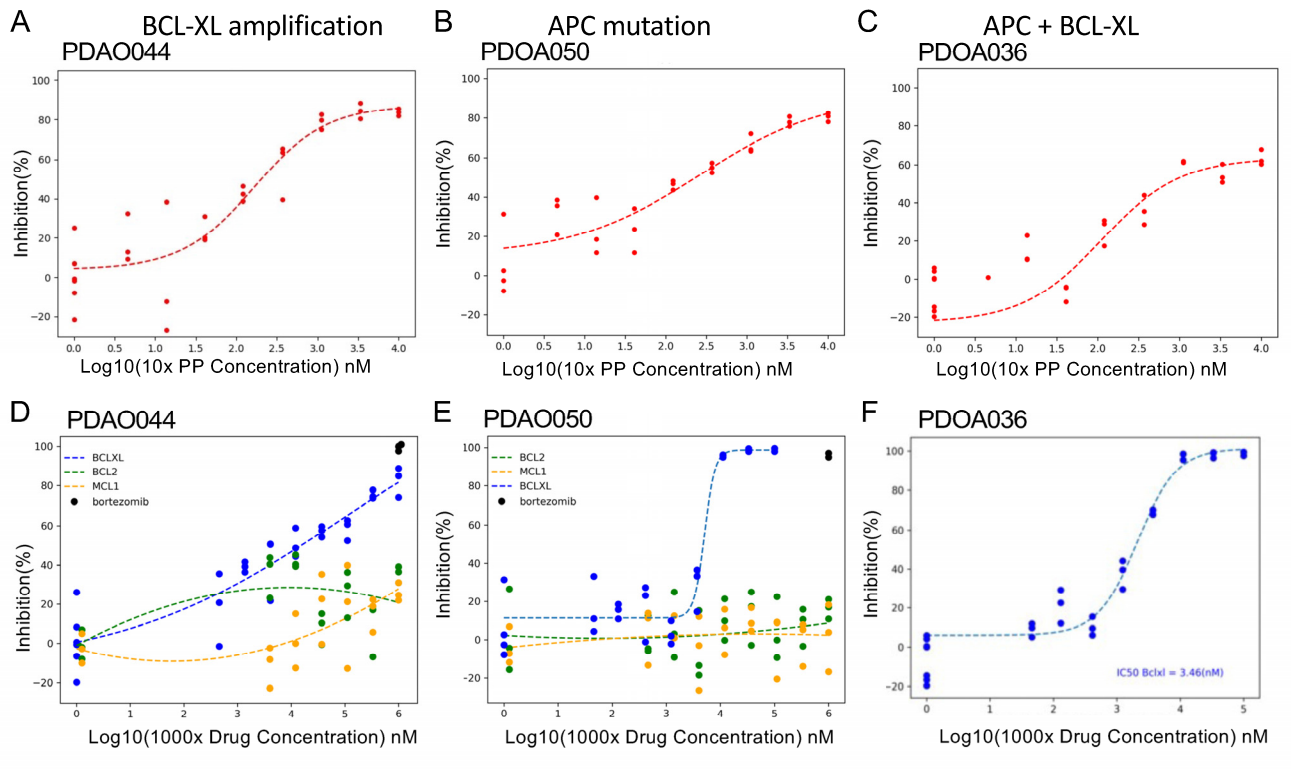

G

Mutation/copy number status	patient	IC50 PP μM	IC50 BCL-XL nM
APC mutation/loss+*BCL-XL* gain	PDAO036	13.11 ± 6.93	3.26 ± 0.51
	PDAO051	72.25 ± 27.35	5.60 ± 0.73
	PDAO056	68.36 ± 30.76	10.66 ± 0.20
	PDAO057	36.87 ± 25.13	8.73 ± 1.85
BCL-XL gain	PDAO044	120.77 ± 64.39	5.44 ± 2.46
APC mutation/loss	PDAO045	97.95 ± 33.95	5.72 ± 3.06
	PDAO050	110.03 ± 45.18	2.05 ± 0.71
	PDAO053	151.35 ± 39.75	6.73 ± 0.46

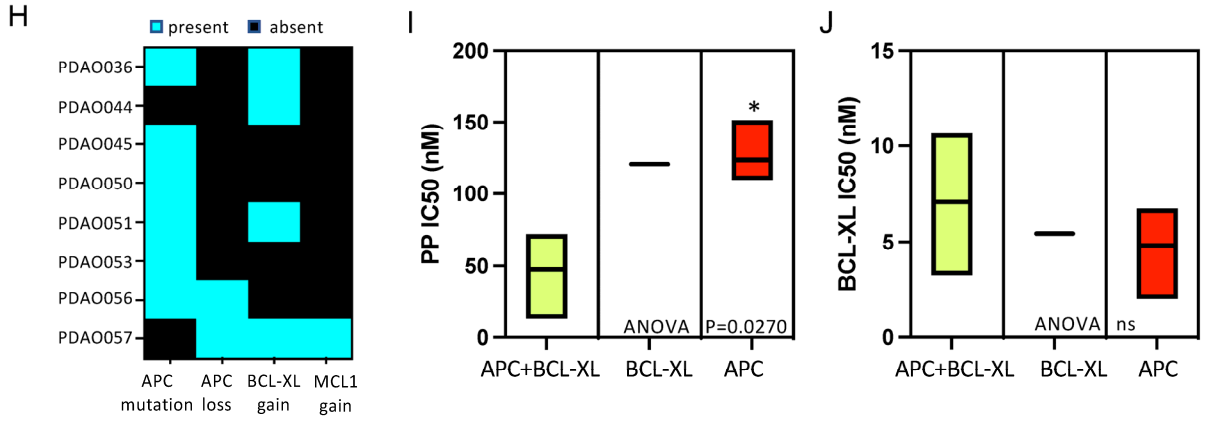

Figure 3. Adenoma cell growth is sensitive to Wnt and BCL-XL inhibitors. (**A**–**C**) Dose–response curves for the Wnt inhibitor pyrvinium pamoate (PP) tested against patient-derived adenoma organoids with *BCL-XL* amplification (**A**), *APC* mutation (**B**), and *APC* loss and *BCL-XL* amplification (**C**). Concentration of the compound is plotted on a log scale (x-axis) against the percent inhibition of cell growth (inhibition (%)) (y-axis). Individual values from triplicate measurements are plotted and are representative of at least $n = 3$ experiments. (**D**–**F**) Dose–response curves for the pro-apoptotic BCL-XL inhibitor tested against patient-derived adenoma organoids with *BCL-XL* amplification (**D**), *APC* mutation (**E**), and *APC* loss and *BCL-XL* amplification (**F**). Dose–response

curves for pro-apoptotic BCL2 and MCL1 inhibitors are included for PDAO044 (**D**) and PDAO050 (**E**). The concentration of the compound is plotted on a log scale (x-axis) against the percent inhibition (y-axis). Individual values from triplicate measurements are plotted and are representative of at least $n = 3$ experiments. Bortezomib was used as a positive death control. Four-parameter linear regression was used to fit dose–response curves. (**G**) PP and BCL-XL inhibitor IC50 values for PDAO samples. Shown are mean ± SEM, $n > 3$. (**H**) Representation of pathogenic variants and DNA copy number changes for APC mutation, APC loss, BCL-XL amplification, and MCL-1 amplification for individual patient adenoma samples. Samples are arranged in rows with gene mutation, loss, or amplification (gain) shown in columns. (**I**,**J**) Multiple comparison analysis of patient-derived adenoma organoid genetic alterations and response to PP (**I**) and BCL-XL (**J**). Floating bars display the mean, minimum, and maximum values. Significance was determined by a one-way ANOVA test performed with the Bonferroni correction method for multiple comparisons. The ANOVA summary *p*-value is reported on the graph, and the stars above the sample data indicate the multiple comparison adjusted *p*-value, * $p = 0.0270$ for APC+BCL-XL ($n = 4$) and APC ($n = 3$); ns, not significant.

We tested whether the sensitivity of patient-derived adenomas to Wnt (PP) and BCL-XL inhibition led to an effective combination therapy in Wnt-driven colon adenomas (Figures 4 and S9). Dose–response curves for PP, in the absence or presence of titrated BCL-XL, for each of the PDAO lines showed improved sensitivity to PP in the presence of BCL-XL inhibition, even at low concentrations of both drugs (Figures 4A and S9). As with drug assays with single compounds, there was no difference between the early and later passage of adenoma organoids upon treatment with the combination. PDAOs harbouring APC mutations showed profound sensitivity to the PP:BCL-XL inhibitor combination. PDAO044 with *BCL-XL* amplification and no Wnt pathway gene mutation required higher levels of the BCL-XL inhibitor, and the response to PP was still improved with the addition of the BCL-XL inhibitor; however, this subtype was limited to a single sample (Figure 4A). PDAO045, which has an APC mutation, appeared to be the most sensitive to the drug combination, with 100% inhibition at 3.7 nM BCL-XL inhibitor and 0.457 nM PP (Figure S9). Bliss scores were calculated for each combination and indicate potent synergistic inhibition, particularly in *APC* mutant cells, highlighted in red on the heatmap (Figures 4B and S9). A Bliss score greater than 10 is indicative of a synergistic interaction between the two drugs. *APC* mutant PDAO050 showed a high degree of synergy at the lowest doses of the BCL-XL inhibitor (Figure 4B). PDAO036 harbouring both an *APC* mutation and *BCL-XL* amplification also showed strong synergistic interactions, whereas PDAO044 with *BCL-XL* amplification alone did not show the same high degree of synergy (Figure 4B). Notably, PDAO samples with an *APC* mutation with or without *BCL-XL* amplification all showed potent synergy (Figure S9A–E). Multiple comparison analysis of PDAO *APC* mutations and *BCL-XL* copy number increase and response to PP in combination with BCL-XL inhibition demonstrated the increased potency with the combination seen above but did not reveal any differences between the groups (Figure 4C). We tested the combination of PP and BCL-XL inhibitors on organoids established from normal colon or non-tumour adenoma margin tissue, and there was reduced sensitivity compared to adenoma organoids (Figures 4D and S10). These data demonstrate that treatment with combined PP and BCL-XL inhibitors resulted in reduced adenoma organoid growth.

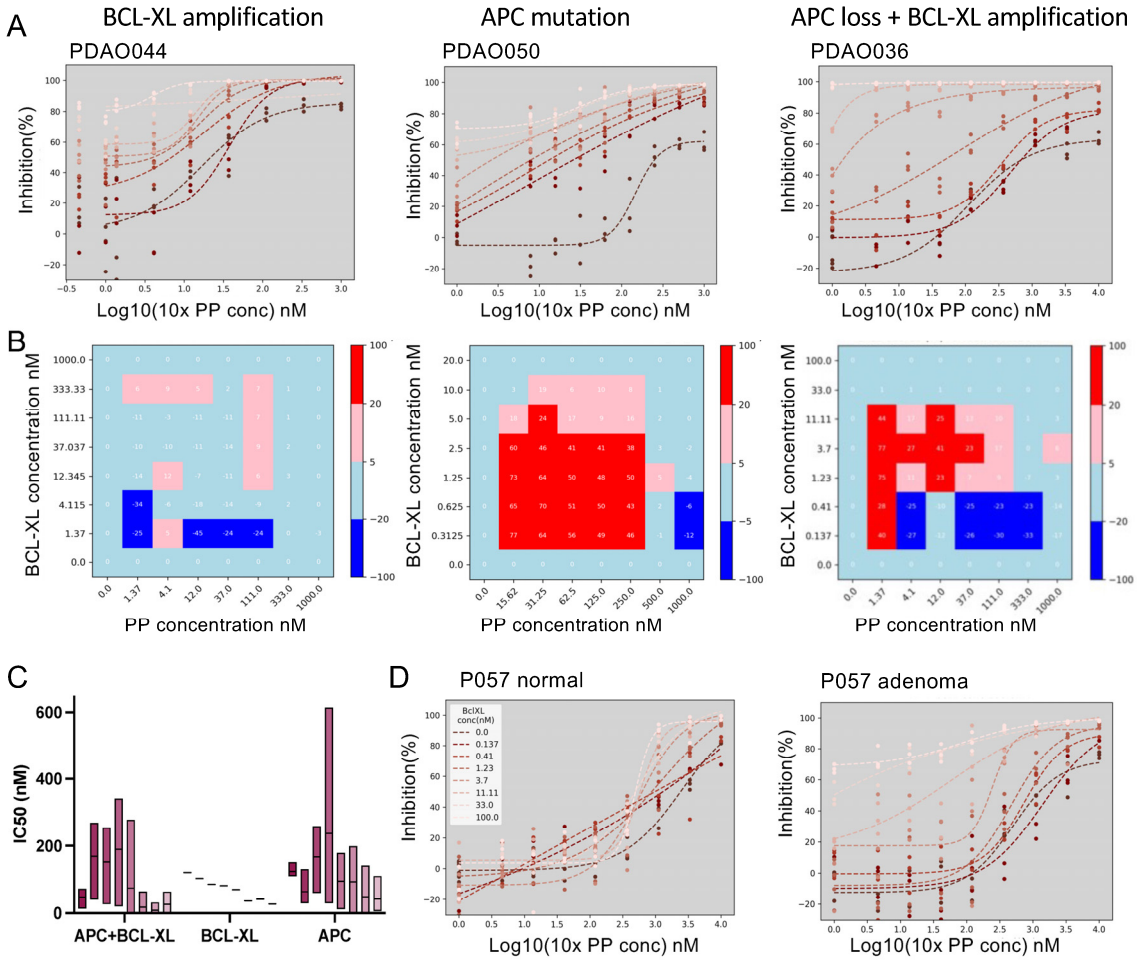

Figure 4. Synergy of combined Wnt and BCL-XL inhibitors in Wnt-driven PDAO. (**A**) Dose–response curves for the Wnt inhibitor pyrvinium pamoate (PP) with BCL-XL inhibitor titration against patient-derived adenoma organoids with *BCL-XL* amplification (**left**), *APC* mutation (**middle**), and *APC* loss and *BCL-XL* amplification (**right**). The concentration of PP is plotted on a log scale (x-axis) against the percent inhibition of cell growth (inhibition (%)) (y-axis) and BCL-XL inhibitor concentration coloured from light to dark with increasing BCL-XL concentration (0, 0.14, 0.41, 1.23, 3.70, 11.11, 33.0, 100 nM BCL-XL). Individual values from triplicate measurements are plotted and are representative of at least $n = 3$ experiments. Four-parameter linear regression was used to fit dose–response curves. Significance was determined using the R package "drc", PDAO044 $p < 0.005$ at 33, and 100.0 nM BCL-XL; PDAO050 $p < 0.05$ at 3.7 nM, $p < 0.001$ at 33, and 100 nM BCL-XL. (**B**) Bliss synergy heatmaps for patient-derived adenoma organoids with *BCL-XL* amplification (**left**), *APC* mutation (**middle**), and *APC* loss and *BCL-XL* amplification (**right**) treated with distinct combinations of Wnt (x-axis) and BCL-XL (y-axis) inhibitors ranging from 0 to 1 µM. The heatmap represents the Bliss score coloured according to the scale, from 100 (high degree of synergy, red) to −100 (low degree of synergy, blue). (**C**) Multiple comparison analysis of patient-derived adenoma organoid genetic alterations and response to PP in combination with increasing concentrations of the BCL-XL inhibitor. Floating bars display the mean, minimum, and maximum values. (**D**) Organoids derived from normal tissue are less sensitive to the PP and BCL-XL inhibitor combination compared to adenoma organoids. Dose–response curves for the Wnt inhibitor pyrvinium pamoate (PP) with BCL-XL inhibitor titration against patient-derived organoids from normal colon (**left**) and adenoma (**right**) tissue, as in (**A**). Normal colon, not significant, adenoma $p < 0.05$ at 33, 100 nM BCL-XL.

3.4. Combination of PP and BCL-XL Induces Apoptosis in Adenoma Organoids

PDAOs were treated with PP or the BCL-XL inhibitor as single agents or in combination, and apoptosis was evaluated by fluorescence microscopy (Figure 5, Supplemental Movie S4). Hoechst was used to stain all nuclei, whereas Annexin V and TO-PRO-3 were

used to mark apoptotic and dead cells, respectively. There was no evidence of Annexin V binding or TO-PRO-3 uptake in vehicle-treated PDAOs (Figure 5, Supplemental Movie S4). Similarly, after 5 h of treatment with PP (1 μM), there was negligible staining with Annexin V, and little-to-no cell death was observed with TO-PRO-3 staining (Figure 5A, Supplemental Movie S4). However, there was pronounced apoptotic cell death in PDAOs treated with BCL-XL (0.1 μM) as a single agent, but cell death was increased significantly when the organoids were treated with BCL-XL in the presence of PP (1 μM) (Figure 5). Thus, the combination of the Wnt inhibitor PP and BCL-XL inhibition results in the potent synergistic apoptotic killing of PDAOs.

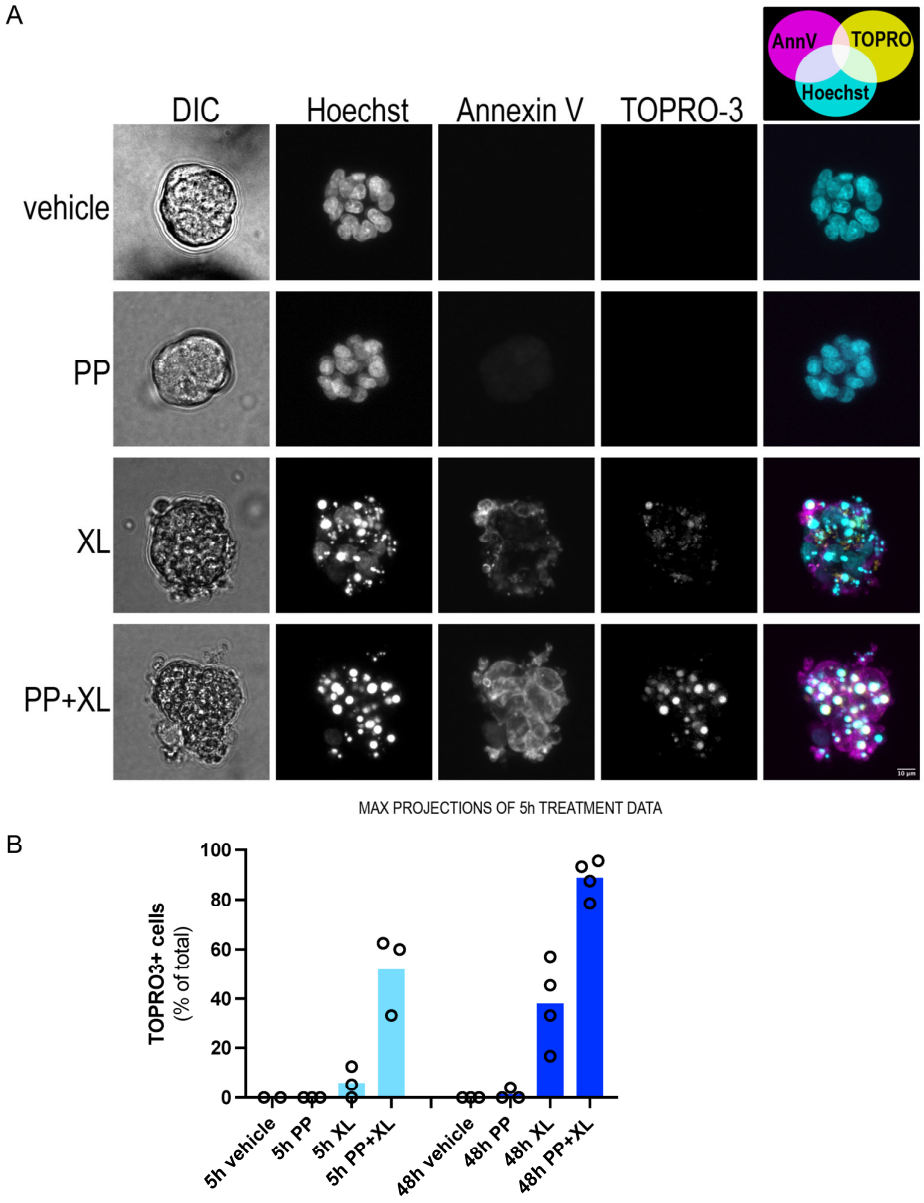

Figure 5. Combination of Wnt and BCL-XL inhibition results in apoptosis. (**A**) Patient-derived adenoma organoids (P044Ad) were treated with vehicle, PP, BCL-XL (XL), or PP+BCL-XL (PP+XL), and Hoechst (blue), Annexin V (magenta), and TOPRO-3 (yellow) uptake were measured via DIC and 3D confocal microscopy at 5 h. Intense Annexin V (apoptosis) and TOPRO-3 (cell death) are evident in BCL-XL and PP+BCL-XL Z-stack projections. Scale bar: 10 μm. (**B**) Quantitation of cell death (TOPRO+ cells) at 5 h and 48 h treatments with vehicle, PP, PBC-XL (XL), or PP+BCL-XL (PP+XL). Shown are mean %TOPRO+ cells (N > 23 cells/point); $p = 0.0007$ at 5 h and $p < 0.0001$ at 48 h. Ordinary one-way ANOVA using GraphPad PrismVer9 and Tukey's multiple comparison test.

4. Discussion

In this study, we have demonstrated that the combination of an FDA-approved Wnt signalling inhibitor (PP) with the pro-apoptotic mimetic compound (A-1331852) acts synergistically to kill patient-derived colon adenoma organoids. In a previous report, we explored the utility of combining the Wnt signalling inhibitor PP with the BCL-2 family inhibitor ABT737/263 in killing CRC cells harbouring *APC* mutations [21]. We found that the PP/ABT263 combination killed the APC-defective cancer cells both in vitro and in tumour xenografts in vivo [21]. Here, we tested small molecules that specifically inhibit BCL-2, BCL-XL, or MCL-1 and discovered that only the inhibition of BCL-XL was effective in inducing cell death in patient-derived colon adenoma organoids, similar to previously published reports [39]. We established a cohort of colon adenomas in organoid culture from different patients to provide a relevant model for testing targeted therapies. We propose that a combination of molecules that target Wnt signalling and promote cell death provide a tractable approach for killing pre-cancerous adenoma cells, thus preventing the development of colon cancer.

The overall features of the adenoma organoids recapitulated the morphology and differentiation state of the primary adenoma tissue from which they were derived. This is consistent with previous reports on organoids derived from normal colon and patient-derived colorectal cancers that maintain the structure and cellular organisation of the original tissue [33,34,40,41]. The histological features of the primary tissue were evident in the organoids along with the maintenance of a proliferative compartment via Ki67 staining, indicating continuous growth in culture. The epithelial architecture and polarity of colon crypt structures were maintained in the adenoma organoids, which produced multiple budding structures, similar to the normal colon [33]. However, we noted that several organoid crypt buds displayed an inverted phenotype with apical membranes exposed, which may be a feature of crypt production in adenoma organoids, as has been reported for organoid cultures from inflammatory bowel disease patients [42]. Importantly, we now show that patient-derived adenoma organoids can be used to trial therapies and provide a new prevention strategy to target the adenoma cells at an early stage of CRC. Responses of patient-derived adenoma organoids to drug combinations may also provide a basis for predicting patient responses, as emerging studies now show for a number of cancer types [40,43–45].

As we have previously shown that a combination of a Wnt signalling antagonist with a pro-apoptotic small molecule compound can kill CRC cells [21], we extended this approach to targeting colon adenoma cells. WES revealed that most colon adenomas contained an *APC* mutation or loss of function, and we predicted that colon adenoma organoids would be sensitive to Wnt signalling inhibition. The copy number gain or mutation of *KRAS* was also evident in the majority of adenomas in the cohort, and one sample with no alteration in APC and KRAS instead had a gain of *BCL2L1* (BCL-XL). Of the Wnt inhibitors tested, only PP was effective for inhibiting the growth of the adenoma organoids. While it was not surprising that IWP2 was not effective, given that its proposed mechanism of action is upstream of APC [24], it was surprising that tankyrase inhibition did not reduce adenoma cell growth. We note there was a slight effect of the tankyrase inhibitor in APC-deficient cells, but in contrast to PP, tankyrase inhibitors are not effective in all APC mutant cells [28]. PP is reported to inhibit other signalling pathways in addition to Wnt, including the inhibition of mitochondrial function in myeloma, lymphoma, and pancreatic cancer cells [16,17,19,46,47]. How PP inhibits mitochondria is not completely understood. Earlier studies implicated the mitochondrial respiratory complex [16]; however, PP has more recently been shown to inhibit mitochondrial oxidative phosphorylation more broadly [47]. In our adenoma cultures, PP was effective in inhibiting cell growth, particularly in cells with a mutation or

loss of *APC*. PP has been shown to inhibit Wnt signalling by the activation of CK1a [13] and, recently, by attenuating the degradation of CK1a [48]. While the detailed mechanism of action of PP in adenoma cells remains to be fully elucidated, as an FDA-approved compound, it has undergone extensive characterisation with regard to pharmacokinetic and toxicity properties, making it a tractable candidate for killing adenomas.

BCL-XL has been reported as the primary survival factor in CRC [38], so it was not surprising that its inhibition resulted in the potent killing of adenoma organoid cells. Unlike the study with CRC patient-derived organoids [38], we did not see an effect of the MCL-1 inhibitor, suggesting that targeting BCL-XL is sufficient to induce colon adenoma cell death. However, Ramesh et al. [39] demonstrated that BCL-XL inhibition impaired the growth of adenomas in vivo and enhanced cell death in tumour-derived organoids, in particular in adenomas harbouring APC mutations. MCL-1 inhibition did not affect adenoma growth, which is consistent with the data reported here. We did not test the combination of BCL-XL and MCL-1 inhibitors; instead, we combined a BCL-XL inhibitor with PP (Wnt inhibitor). This combination demonstrated potent synergistic killing, irrespective of *KRAS* alterations. Furthermore, when combined, the IC50 of PP inhibition was found to decrease in the presence of BCL-XL inhibition, and the IC50 of BCL-XL inhibition decreases in the presence of PP. Notably, organoids established from normal tissue were not sensitive to the combination. Thus, combining these agents allows for lower doses of the BCL-XL inhibitor and PP to be used for killing adenoma cells. The ability to reduce the dose of the BCL inhibitor is particularly important because of the toxicities associated with the BCL-2 family targeted therapies, limiting their use in clinical settings [49,50]. Clinical studies in lymphoid malignancies have demonstrated patient benefits with BCL-2 inhibition; however, high doses resulted in thrombocytopenia as a result of BCL-XL inhibition [51]. Similarly, when a BCL-2 inhibitor was administered in combination with chemotherapeutic agents in patients with solid tumours, higher levels of neutropenia were observed than when chemotherapy was used alone in some patients [52]. A recent phase I trial of BH3-mimetic drugs, venetoclax (BCL-2 inhibitor), with low-dose navitoclax (BCL-XL inhibitor), in combination with chemotherapy in patients with acute lymphoblastic leukemia or lymphoblastic lymphomas, was well tolerated, demonstrating promising utility for low-dose BCL-XL inhibitor agents [53]. Studies on the efficacy of BCL-2 and BCL-XL inhibitors in colorectal cancer have been limited, and to date, only venetoclax has been approved for the treatment of solid tumours [54]. It is possible that the use of BCL inhibitors alone is less efficacious in solid tumours due to the complex microenvironment. Whilst promising results are emerging in preclinical settings, testing combination therapies is challenging, and the clinical potential is yet to be shown.

5. Conclusions

This study demonstrates that the combination of PP and BCL-XL inhibitors induces apoptosis in colorectal adenoma cells with different combinations of *APC*, *KRAS*, and *BCL-XL* mutations and copy number variations. There are several limitations to the study. While the sample size is small, we show potent synergistic killing in all adenoma samples tested, suggesting that the new drug combination tested here would be expected to be beneficial for the removal of adenoma cells. We note that there was only one sample with a gain of *BCL-XL* and no Wnt pathway mutation, so the interpretation of differences in drug response should be treated cautiously. We did not explore the effects of immune components, and while there are few reports of immune system involvement in the formation or progression of adenomas, the involvement of the immune system in adenoma killing is worthy of further investigation. The combination treatment resulted in synergistic effects and a profound induction of apoptosis compared to individual drug treatments. Future work

using PDXs from adenoma organoids will be important to measure the toxicity of the drug combinations in an in vivo setting. Our findings provide the basis for new approaches to colon cancer prevention, and the testing of patient-derived organoids from pre-cancerous stages provides an opportunity for identifying anti-cancer drug combinations likely to improve outcomes for patients.

Supplementary Materials: The following supporting information can be downloaded at: https://www.mdpi.com/article/10.3390/organoids4030015/s1, Figure S1: Patient-derived colon adenoma organoids recapitulate the histological features of their primary adenoma tissue; Figure S2: Structural organization of patient-derived colon adenoma organoids; Figure S3: Genetic alteration of patient adenoma samples; Figure S4: Absence of APC and K-RAS mutations in patient normal colon samples; Figure S5: Copy number alterations of patient adenoma samples; Figure S6: Copy number alterations of patient adenoma samples; Figure S7: Adenoma cell growth is sensitive to Wnt and BCL-XL inhibitors; Figure S8: Adenoma cell growth sensitivity to Wnt inhibitors; Figure S9: Synergy of combined Wnt and BCL-XL inhibitors in Wnt-driven PDAO; Figure S10: Organoids derived from normal colon or adenoma margin tissue show reduced sensitivity to the PP and BCL-XL combination; Table S1: Passage number of PDAO cultures in drug assays; Movie S1: Immunostained PDAOs display properly organised intestinal cell layers; Movie S2: Immunostained PDAOs display properly organised intestinal cell layers; Movie S3: Immunostained PDAOs display properly organised intestinal cell layers; Movie S4: Representative 3-dimensional confocal images of PDAOs after 5 h of treatment.

Author Contributions: M.C.F., S.R.K., A.S., Y.H. and I.P. performed the experiments. G.B. and R.S. were responsible for recruiting the patients and providing the clinical data and samples for the generation of organoids. M.C.F., S.R.K., K.Y.C.F., L.C. and C.M. were responsible for generating the genomic sequencing data. M.C. reported on the pathology of the adenoma tissue and organoids. A.W.B. and M.C.F. guided the design and interpretation of the experiments and wrote the first draft of the manuscript. All authors have read and agreed to the published version of the manuscript.

Funding: This work was supported generously by WEHI and the Ludwig Institute for Cancer Research and NH&MRC program grant #487922.

Institutional Review Board Statement: This study was conducted in accordance with the Declaration of Helsinki, and the NH&MRC Statement on Ethical Conduct in Human Research and protocol was approved by The Alfred Health Human Research Ethics Committee (LR195-14, approved 29 April 2014), the Walter and Eliza Hall Institute Human Research Ethics Committee (HREC14/17, approved 15 December 2014.), and the Central Adelaide Local Health Network Human Research Ethics Committee (HREC/19/CALHN/13, approved 31 January 2019).

Informed Consent Statement: All patients provided informed consent.

Data Availability Statement: Data is available upon request in accordance with patient confidentiality surrounding whole genome sequencing and patient clinical data.

Acknowledgments: The authors acknowledge the colorectal colonoscopy team at the Epworth Hospital, Richmond, Alfred Health, and Lyell McEwin Hospital for their contribution to tissue collection as well as the collation of patient data. The authors acknowledge the contribution of Robyn Secomb and Helen Chen for their assistance with patient informed consent and the collection of adenoma samples at the Epworth Hospital. The authors acknowledge the patients for consenting to the study and providing tissue samples. The authors acknowledge Theodora Almond for her assistance in culturing and the biobank of patient-derived organoids used for this study and Dana Pascovici for critically reviewing the manuscript.

Conflicts of Interest: The authors declare no conflicts of interest.

References

1. Arnold, M.; Sierra, M.S.; Laversanne, M.; Soerjomataram, I.; Jemal, A.; Bray, F. Global patterns and trends in colorectal cancer incidence and mortality. *Gut* **2017**, *66*, 683–691. [CrossRef] [PubMed]
2. Kinzler, K.W.; Vogelstein, B. Landscaping the cancer terrain. *Science* **1998**, *280*, 1036–1037. [CrossRef] [PubMed]
3. Kinzler, K.W.; Nilbert, M.C.; Su, L.-K.; Vogelstein, B.; Bryan, T.M.; Levy, D.B.; Smith, K.J.; Preisinger, A.C.; Hedge, P.; McKechnie, D.; et al. Identification of FAP locus genes from chromosome 5q21. *Science* **1991**, *253*, 661–665. [CrossRef] [PubMed]
4. Shaukat, A.; Kaltenbach, T.; Dominitz, J.A.; Robertson, D.J.; Anderson, J.C.; Cruise, M.; Burke, C.A.; Gupta, S.; Lieberman, D.; Syngal, S.; et al. Endoscopic Recognition and Management Strategies for Malignant Colorectal Polyps: Recommendations of the US Multi-Society Task Force on Colorectal Cancer. *Gastrointest. Endosc.* **2020**, *92*, 997–1015.e1. [CrossRef]
5. Wang, L.; He, X.; Ugai, T.; Haruki, K.; Lo, C.-H.; Hang, D.; Akimoto, N.; Fujiyoshi, K.; Wang, M.; Fuchs, C.S.; et al. Risk Factors and Incidence of Colorectal Cancer According to Major Molecular Subtypes. *JNCI Cancer Spectr.* **2021**, *5*, pkaa089. [CrossRef]
6. Delisle, M.; Helewa, R.M.; Ward, M.A.R.; Hochman, D.J.; Park, J.; McKay, A. The Association Between Wait Times for Colorectal Cancer Treatment and Health Care Costs: A Population-Based Analysis. *Dis. Colon Rectum* **2020**, *63*, 160–171. [CrossRef]
7. Nusse, R.; Clevers, H. Wnt/beta-Catenin Signaling, Disease, and Emerging Therapeutic Modalities. *Cell* **2017**, *169*, 985–999. [CrossRef]
8. Cottrell, S.; Bicknell, D.; Kaklamanis, L.; Bodmer, W. Molecular analysis of APC mutations in familial adenomatous polyposis and sporadic colon carcinomas. *Lancet* **1992**, *340*, 626–630. [CrossRef]
9. Sugai, T.; Habano, W.; Takagi, R.; Yamano, H.; Eizuka, M.; Arakawa, N.; Takahashi, Y.; Yamamoto, E.; Kawasaki, K.; Yanai, S.; et al. Analysis of molecular alterations in laterally spreading tumors of the colorectum. *J. Gastroenterol.* **2017**, *52*, 715–723. [CrossRef]
10. Sugimoto, T.; Ohta, M.; Ikenoue, T.; Yamada, A.; Tada, M.; Fujishiro, M.; Ogura, K.; Yamaji, Y.; Okamoto, M.; Kanai, F.; et al. Macroscopic morphologic subtypes of laterally spreading colorectal tumors showing distinct molecular alterations. *Int. J. Cancer* **2010**, *127*, 1562–1569. [CrossRef]
11. Bettington, M.; Walker, N.; Clouston, A.; Brown, I.; Leggett, B.; Whitehall, V. The serrated pathway to colorectal carcinoma: Current concepts and challenges. *Histopathology* **2013**, *62*, 367–386. [CrossRef] [PubMed]
12. Weisenberger, D.J.; Siegmund, K.D.; Campan, M.; Young, J.; Long, T.I.; Faasse, M.A.; Kang, G.H.; Widschwendter, M.; Weener, D.; Buchanan, D.; et al. CpG island methylator phenotype underlies sporadic microsatellite instability and is tightly associated with BRAF mutation in colorectal cancer. *Nat. Genet.* **2006**, *38*, 787–793. [CrossRef] [PubMed]
13. Thorne, C.A.; Hanson, A.J.; Schneider, J.; Tahinci, E.; Orton, D.; Cselenyi, C.S.; Jernigan, K.K.; Meyers, K.C.; Hang, B.I.; Waterson, A.G.; et al. Small-molecule inhibition of Wnt signaling through activation of casein kinase 1alpha. *Nat. Chem. Biol.* **2010**, *6*, 829–836. [CrossRef]
14. Momtazi-Borojeni, A.A.; Abdollahi, E.; Ghasemi, F.; Caraglia, M.; Sahebkar, A. The novel role of pyrvinium in cancer therapy. *J. Cell Physiol.* **2018**, *233*, 2871–2881. [CrossRef]
15. Zhang, C.; Zhang, Z.; Zhang, S.; Wang, W.; Hu, P. Targeting of Wnt/beta-Catenin by Anthelmintic Drug Pyrvinium Enhances Sensitivity of Ovarian Cancer Cells to Chemotherapy. *Med. Sci. Monit.* **2017**, *23*, 266–275. [CrossRef]
16. Harada, Y.; Ishii, I.; Hatake, K.; Kasahara, T. Pyrvinium pamoate inhibits proliferation of myeloma/erythroleukemia cells by suppressing mitochondrial respiratory complex I and STAT3. *Cancer Lett.* **2012**, *319*, 83–88. [CrossRef]
17. Xiao, M.; Zhang, L.; Zhou, Y.; Rajoria, P.; Wang, C. Pyrvinium selectively induces apoptosis of lymphoma cells through impairing mitochondrial functions and JAK2/STAT5. *Biochem. Biophys. Res. Commun.* **2016**, *469*, 716–722. [CrossRef]
18. Deng, L.; Lei, Y.; Liu, R.; Li, J.; Yuan, K.; Chen, Y.; Liu, Y.; Lu, Y.; Edwards, C.K., III; Huang, C.; et al. Pyrvinium targets autophagy addiction to promote cancer cell death. *Cell Death Dis.* **2013**, *4*, e614. [CrossRef]
19. Li, B.; Fei, D.L.; Flaveny, C.A.; Dahmane, N.; Baubet, V.; Wang, Z.; Bai, F.; Pei, X.-H.; Rodriguez-Blanco, J.; Hang, B.; et al. Pyrvinium attenuates Hedgehog signaling downstream of smoothened. *Cancer Res.* **2014**, *74*, 4811–4821. [CrossRef]
20. Feng, J.; Jiang, W.; Liu, Y.; Huang, W.; Hu, K.; Li, K.; Chen, J.; Ma, C.; Sun, Z.; Pang, X. Blocking STAT3 by pyrvinium pamoate causes metabolic lethality in KRAS-mutant lung cancer. *Biochem. Pharmacol.* **2020**, *177*, 113960. [CrossRef]
21. Corona, S.P.; Walker, F.; Weinstock, J.; Lessene, G.; Faux, M.; Burgess, A.W. Dual drug targeting to kill colon cancers. *Cancer Med.* **2022**, *11*, 2612–2626. [CrossRef] [PubMed]
22. Faux, M.C.; Weinstock, J.; Gogos, S.; Prato, E.; Azimpour, A.I.; O'Keefe, R.; Cathcart-King, Y.; Garnham, A.L.; Ernst, M.; Preaudet, A.; et al. Combined Treatment with a WNT Inhibitor and the NSAID Sulindac Reduces Colon Adenoma Burden in Mice with Truncated APC. *Cancer Res. Commun.* **2022**, *2*, 66–77. [CrossRef] [PubMed]
23. Schatoff, E.M.; Goswami, S.; Zafra, M.P.; Foronda, M.; Shusterman, M.; Leach, B.I.; Katti, A.; Diaz, B.J.; Dow, L.E. Distinct Colorectal Cancer–Associated APC Mutations Dictate Response to Tankyrase Inhibition. *Cancer Discov.* **2019**, *9*, 1358–1371. [CrossRef] [PubMed]
24. Chen, B.; Dodge, M.E.; Tang, W.-J.; Lu, J.; Ma, Z.; Fan, C.-W.; Wei, S.; Hao, W.; Kilgore, J.; Williams, N.S.; et al. Small molecule-mediated disruption of Wnt-dependent signaling in tissue regeneration and cancer. *Nat. Chem. Biol.* **2009**, *5*, 100–107. [CrossRef]

25. Yip, H.Y.K.; Tan, C.W.; Hirokawa, Y.; Burgess, A.W. Colon organoid formation and cryptogenesis are stimulated by growth factors secreted from myofibroblasts. *PLoS ONE* **2018**, *13*, e0199412. [CrossRef]
26. Hirokawa, Y.; Clarke, J.; Palmieri, M.; Tan, T.; Mouradov, D.; Li, S.; Lin, C.; Li, F.; Luo, H.; Wu, K.; et al. Low-viscosity matrix suspension culture enables scalable analysis of patient-derived organoids and tumoroids from the large intestine. *Commun. Biol.* **2021**, *4*, 1067. [CrossRef]
27. Dekkers, J.F.; Alieva, M.; Wellens, L.M.; Ariese, H.C.R.; Jamieson, P.R.; Vonk, A.M.; Amatngalim, G.D.; Hu, H.; Oost, K.C.; Snippert, H.J.G.; et al. High-resolution 3D imaging of fixed and cleared organoids. *Nat. Protoc.* **2019**, *14*, 1756–1771. [CrossRef]
28. Lau, T.; Chan, E.; Callow, M.; Waaler, J.; Boggs, J.; Blake, R.A.; Magnuson, S.; Sambrone, A.; Schutten, M.; Firestein, R.; et al. A novel tankyrase small-molecule inhibitor suppresses APC mutation-driven colorectal tumor growth. *Cancer Res.* **2013**, *73*, 3132–3144. [CrossRef]
29. Moré, J.J.; Garbow, B.S.; Hillstrom, K.E. *User Guide for Minpack-1*; CERN: Geneva, Switzerland, 1980.
30. Bliss, C.I. The toxicity of poisons applied jointly. *Ann. Appl. Biol.* **1939**, *26*, 585–615. [CrossRef]
31. Hunter, J.D. Matplotlib: A 2D Graphics Environment. *Comput. Sci. Eng.* **2007**, *9*, 90–95. [CrossRef]
32. Ritz, C.; Baty, F.; Streibig, J.C.; Gerhard, D. Dose-Response Analysis Using R. *PLoS ONE* **2015**, *10*, e0146021. [CrossRef] [PubMed]
33. Sato, T.; Stange, D.E.; Ferrante, M.; Vries, R.G.J.; Van Es, J.H.; Van Den Brink, S.; Van Houdt, W.J.; Pronk, A.; Van Gorp, J.; Siersema, P.D.; et al. Long-term expansion of epithelial organoids from human colon, adenoma, adenocarcinoma, and Barrett's epithelium. *Gastroenterology* **2011**, *141*, 1762–1772. [CrossRef] [PubMed]
34. van de Wetering, M.; Francies, H.E.; Francis, J.M.; Bounova, G.; Iorio, F.; Pronk, A.; van Houdt, W.; van Gorp, J.; Taylor-Weiner, A.; Kester, L.; et al. Prospective derivation of a living organoid biobank of colorectal cancer patients. *Cell* **2015**, *161*, 933–945. [CrossRef] [PubMed]
35. Schultz, C.W.; Nevler, A. Pyrvinium Pamoate: Past, Present, and Future as an Anti-Cancer Drug. *Biomedicines* **2022**, *10*, 3249. [CrossRef]
36. Faux, M.C.; King, L.E.; Kane, S.R.; Love, C.; Sieber, O.M.; Burgess, A.W. APC regulation of ESRP1 and p120-catenin isoforms in colorectal cancer cells. *Mol. Biol. Cell* **2021**, *32*, 120–130. [CrossRef]
37. Schwab, R.H.M.; Amin, N.; Flanagan, D.J.; Johanson, T.M.; Phesse, T.J.; Vincan, E. Wnt is necessary for mesenchymal to epithelial transition in colorectal cancer cells. *Dev. Dyn.* **2018**, *247*, 521–530. [CrossRef]
38. Luo, M.-J.; Palmieri, M.; Riffkin, C.D.; Sakthianandeswaren, A.; Djajawi, T.M.; Hirokawa, Y.; Shuttleworth, V.; Segal, D.H.; White, C.A.; Nhu, D.; et al. Defining the susceptibility of colorectal cancers to BH3-mimetic compounds. *Cell Death Dis.* **2020**, *11*, 735. [CrossRef]
39. Ramesh, P.; Lannagan, T.R.M.; Jackstadt, R.; Taboada, L.A.; Lansu, N.; Wirapati, P.; van Hooff, S.R.; Dekker, D.; Pritchard, J.; Kirov, A.B.; et al. BCL-XL is crucial for progression through the adenoma-to-carcinoma sequence of colorectal cancer. *Cell Death Differ.* **2021**, *28*, 3282–3296. [CrossRef]
40. Vlachogiannis, G.; Hedayat, S.; Vatsiou, A.; Jamin, Y.; Fernández-Mateos, J.; Khan, K.; Lampis, A.; Eason, K.; Huntingford, I.; Burke, R.; et al. Patient-derived organoids model treatment response of metastatic gastrointestinal cancers. *Science* **2018**, *359*, 920–926. [CrossRef]
41. Tan, T.; Mouradov, D.; Lee, M.; Gard, G.; Hirokawa, Y.; Li, S.; Lin, C.; Li, F.; Luo, H.; Wu, K.; et al. Unified framework for patient-derived, tumor-organoid-based predictive testing of standard-of-care therapies in metastatic colorectal cancer. *Cell Rep. Med.* **2023**, *4*, 101335. [CrossRef]
42. D'aldebert, E.; Quaranta, M.; Sébert, M.; Bonnet, D.; Kirzin, S.; Portier, G.; Duffas, J.-P.; Chabot, S.; Lluel, P.; Allart, S.; et al. Characterization of Human Colon Organoids from Inflammatory Bowel Disease Patients. *Front. Cell Dev. Biol.* **2020**, *8*, 363. [CrossRef] [PubMed]
43. Lee, S.H.; Hu, W.; Matulay, J.T.; Silva, M.V.; Owczarek, T.B.; Kim, K.; Chua, C.W.; Barlow, L.M.J.; Kandoth, C.; Williams, A.B.; et al. Tumor Evolution and Drug Response in Patient-Derived Organoid Models of Bladder Cancer. *Cell* **2018**, *173*, 515–528.e17. [CrossRef] [PubMed]
44. Ooft, S.N.; Weeber, F.; Dijkstra, K.K.; McLean, C.M.; Kaing, S.; Van Werkhoven, E.; Schipper, L.; Hoes, L.; Vis, D.J.; Van De Haar, J.; et al. Patient-derived organoids can predict response to chemotherapy in metastatic colorectal cancer patients. *Sci. Transl. Med.* **2019**, *11*, eaay2574. [CrossRef]
45. Sachs, N.; de Ligt, J.; Kopper, O.; Gogola, E.; Bounova, G.; Weeber, F.; Balgobind, A.V.; Wind, K.; Gracanin, A.; Begthel, H.; et al. A Living Biobank of Breast Cancer Organoids Captures Disease Heterogeneity. *Cell* **2018**, *172*, 373–386.e10. [CrossRef]
46. Dattilo, R.; Mottini, C.; Camera, E.; Lamolinara, A.; Auslander, N.; Doglioni, G.; Muscolini, M.; Tang, W.; Planque, M.; Ercolani, C.; et al. Pyrvinium Pamoate Induces Death of Triple-Negative Breast Cancer Stem-Like Cells and Reduces Metastases Through Effects on Lipid Anabolism. *Cancer Res.* **2020**, *80*, 4087–4102. [CrossRef]
47. Schultz, C.W.; McCarthy, G.A.; Nerwal, T.; Nevler, A.; DuHadaway, J.B.; McCoy, M.D.; Jiang, W.; Brown, S.Z.; Goetz, A.; Jain, A.; et al. The FDA-Approved Anthelmintic Pyrvinium Pamoate Inhibits Pancreatic Cancer Cells in Nutrient-Depleted Conditions by Targeting the Mitochondria. *Mol. Cancer Ther.* **2021**, *20*, 2166–2176. [CrossRef]

48. Shen, C.; Nayak, A.; Neitzel, L.R.; Yang, F.; Li, B.; Williams, C.H.; Hong, C.C.; Ahmed, Y.; Lee, E.; Robbins, D.J. The Casein kinase 1alpha agonist pyrvinium attenuates Wnt-mediated CK1alpha degradation via interaction with the E3 ubiquitin ligase component Cereblon. *J. Biol. Chem.* **2022**, *298*, 102227. [CrossRef]
49. Mason, K.D.; Carpinelli, M.R.; Fletcher, J.I.; Collinge, J.E.; Hilton, A.A.; Ellis, S.; Kelly, P.N.; Ekert, P.G.; Metcalf, D.; Roberts, A.W.; et al. Programmed anuclear cell death delimits platelet life span. *Cell* **2007**, *128*, 1173–1186. [CrossRef]
50. Wang, L.; Doherty, G.A.; Judd, A.S.; Tao, Z.-F.; Hansen, T.M.; Frey, R.R.; Song, X.; Bruncko, M.; Kunzer, A.R.; Wang, X.; et al. Discovery of A-1331852, a First-in-Class, Potent, and Orally-Bioavailable BCL-XL Inhibitor. *ACS Med. Chem. Lett.* **2020**, *11*, 1829–1836. [CrossRef]
51. Wilson, W.H.; O'Connor, O.A.; Czuczman, M.S.; LaCasce, A.S.; Gerecitano, J.F.; Leonard, J.P.; Tulpule, A.; Dunleavy, K.; Xiong, H.; Chiu, Y.-L.; et al. Navitoclax, a targeted high-affinity inhibitor of BCL-2, in lymphoid malignancies: A phase 1 dose-escalation study of safety, pharmacokinetics, pharmacodynamics, and antitumour activity. *Lancet Oncol.* **2010**, *11*, 1149–1159. [CrossRef]
52. Puglisi, M.; van Doorn, L.; Blanco-Codesido, M.; De Jonge, M.J.; Moran, K.; Yang, J.; Busman, T.; Franklin, C.; Mabry, M.; Krivoshik, A.; et al. A phase I safety and pharmacokinetic (PK) study of navitoclax (N) in combination with docetaxel (D) in patients (pts) with solid tumors. *J. Clin. Oncol.* **2011**, *29* (Suppl. 15), 2518. [CrossRef]
53. Pullarkat, V.A.; Lacayo, N.J.; Jabbour, E.; Rubnitz, J.E.; Bajel, A.; Laetsch, T.W.; Leonard, J.; Colace, S.I.; Khaw, S.L.; Fleming, S.A.; et al. Venetoclax and Navitoclax in Combination with Chemotherapy in Patients with Relapsed or Refractory Acute Lymphoblastic Leukemia and Lymphoblastic Lymphoma. *Cancer Discov.* **2021**, *11*, 1440–1453. [CrossRef] [PubMed]
54. Xu, J.; Dong, X.; Huang, D.C.S.; Xu, P.; Zhao, Q.; Chen, B. Current Advances and Future Strategies for BCL-2 Inhibitors: Potent Weapons Against Cancers. *Cancers* **2023**, *15*, 4957. [CrossRef] [PubMed]